The development and early applicationsof the weak-beam technique

Mike Whelan

The development and early applicationsof the weak-beam technique

Journal:	*Philosophical Magazine & Philosophical Magazine Letters*
Manuscript ID:	TPHM-09-Oct-0424
Journal Selection:	Philosophical Magazine
Date Submitted by the Author:	08-Oct-2009
Complete List of Authors:	WHELAN, MIKE; University of Oxford, Materials
Keywords:	electron microscopy, dislocations
Keywords (user supplied):	weak-beam

The development and early applications of the weak-beam technique

M.J. WHELAN
Department of Materials, Parks Road, Oxford, OX1 3PH, UK

Abstract

A short review is given of the way the weak-beam technique for observing dislocations at higher resolution than previously attained was developed, and some of the early applications.

1. Introduction

The advance of scientific research is sometimes accompanied by what might be called 'blind spots', where some possible advance through available knowledge is overlooked until new minds are focussed on the subject. As an example consider the case of Dr. V.E. Cosslett, the leader of the electron microscope group in the Cavendish Laboratory, Cambridge. A graduate of Bristol University, in his early research career he led a somewhat peripatetic existence with fellowships at Bristol, Berlin and London, engaged in electron physics research and endeavouring to lay his hands on the newly developed instrument, the electron microscope, without success. During World War II he was evacuated from Birkbeck College, London, to the Electrical Laboratory of the Physics Department at Oxford, where he was engaged in teaching officer cadets, and where he remained until 1945, when he was advised by the Head of Physics (later Lord Cherwell) that there was no future for him in electron microscopy at Oxford (Mulvey [1]) – an Oxford blind spot! Thereupon he was recruited by Professor Bragg for the Cavendish Laboratory, where he remained for the rest of his career, becoming the father of electron microscopy and associated instrumentation in Cambridge University, and on whom our group in the Cavendish was heavily dependent when we embarked on electron microscope research in 1954.

The development of the weak-beam technique for the study of dislocation distributions at higher resolution than previously attained by conventional bright-field imaging attests to a further example. In 1960 a paper [2] was published calculating the averaged dark-field image profiles of a screw dislocation in a thin crystal using the so-called kinematical theory of diffraction, i.e. when the Bragg diffracted beam is weak (figure 1). At the time this was regarded as a poor approximation to the actual situation pertaining to dislocation images taken in bright-field under strong-beam (dynamical) diffraction conditions. Nevertheless it gave useful information on the visibility criterion depending on n (= $\mathbf{g}.\mathbf{b}$) , where $\mathbf{g}$ is the reciprocal lattice vector of the Bragg reflection and $\mathbf{b}$ is the Burgers vector of the dislocation. What is

clear from figure 1 is that for larger s (the distance of the reciprocal lattice point of the reflection from the Ewald sphere) the dislocation image profile becomes sharper in x (distance on the image). The weak-beam image is sharper than the strong-beam image with the Bragg condition satisfied, where the width is about $\frac{1}{3}\xi_g$, ξ_g being the extinction distance for the Bragg reflection **g** (for notation see reference [3]). For $n = \mathbf{g}.\mathbf{b} = 2$ in figure 1, the half-width of the image is about $1/\pi s$ and the peak is about $1/2\pi s$ from the core of the dislocation. For $s = 2 \times 10^{-2}$ Å^{-1}, the peak is about 8Å from the core, with a half-width about 16Å. A strong-beam image is typically of width about 80Å. To observe such a weak-beam dark-field image in 1960 with the electron microscope available (Elmiskop 1) would have required a goniometer holder for tilting the specimen to an orientation to excite the weak beam, and reliable beam tilting facilities to align the weak beam on the microscope axis. The first was not available, and beam tilting could only be achieved with difficulty, using the mechanical controls designed to align the primary beam on the microscope axis. In addition the possibility of weak-beam imaging was not recognised – the blind spot!

2. The development of the technique

Further advance required the presence of two brilliant research students, David Cockayne and Ian Ray, who joined the author in 1966 following the move of Peter Hirsch's group from Cambridge to Oxford. A problem was suggested to investigate the relation between lattice fringe images and the true position of lattice planes. The long-shot object in mind was to get information about dislocation core structure from fringe images, an object not achieved in a positive sense (see reference [4]). Ray concentrated on experimental technique, while Cockayne carried out calculations on the Oxford KDF9 computer, although eventually he was involved in experimentation also, particularly in achieving the difficult beam tilting with the Elmiskop 1 to align the weak beam with the microscope axis. It is interesting to note that the development did not proceed by recognising the relevance of the kinematical profiles of figure 1. Cockayne carried out many-beam calculations, where the interest was in the lattice fringes at a dislocation formed by the strong beams, but as a by-product a weak beam was seen to have a narrow dislocation image profile. After this the relevance of the old kinematical theory was recognised. The first report of this advance was published in 1969 [5], demonstrating weak-beam imaging of partial dislocations in Cu + 10 at .% Al alloy (figure 2), from which an estimate of stacking fault energy of 10.4 ± 1.8 erg cm^{-2} was derived.

In figure 2 the imaging reflection is **g** = $2\bar{2}0$, and the Burgers vector of the whole dislocation is $\frac{1}{2}[1\bar{1}0]$, which is dissociated into partial dislocations according to

$$\tfrac{1}{2}[1\bar{1}0] \rightarrow \tfrac{1}{6}[1\bar{2}1] + \tfrac{1}{6}[2\bar{1}\bar{1}]$$

The products **g**.**b** for each of these in order are 2, 1 and 1. Many-beam calculations were carried out for this dislocation configuration. An example is shown in figure 3. For a number of computed images the average separations lay within 57 ± 5 Å for $s_g = -2.25x10^{-2}$ Å^{-1} and 100kV electrons, which gave the estimate of stacking fault energy above.

Cockayne et al [5] proposed an approximate condition to determine the position of the weak-beam peak relative to the dislocation core, namely $s_g + (d/dz)(\mathbf{g}.\mathbf{R}) = 0$ at a maximum of $d\mathbf{R}/dz$ along a column of crystal, where **R** is the displacement vector of the dislocation. This corresponds to the maximum tilt of diffracting planes along the column being just sufficient to compensate for *s*, i.e. to tilt to the reflecting position. For a screw dislocation with **b** = $\frac{1}{2}[1\bar{1}0]$ and **g** = $2\bar{2}0$, this leads to a position of the peak at $-1/\pi s$. The kinematical theory curve of figure 1 for $n = \mathbf{g}.\mathbf{b} = 2$ has a peak at about $-1/2\pi s$. Evidently the kinematical theory leads to a peak where the tilt over-compensates for *s*. A detailed discussion has been given by Cockayne [6], where many-beam calculations show that the actual peak may lie between these two values depending on the depth of the dislocation.

Figure 4 illustrates schematically some geometries which have been used for weak-beam imaging. In figure 4(a) the reciprocal lattice point **g** is on the Ewald sphere, and the weak-beam image (broken line) is taken in –**g**, as in figure 2 where **g** = $\bar{2}20$. However, it can be shown from symmetry considerations that the same weak-beam image results if only the incident beam (and not the specimen) is tilted, so that 3 **g** is strongly excited (figure 4(b)). But in practice it is best to try to achieve a situation where no diffracted beam is strongly excited as shown schematically in figure 4(c), a situation approximating to kinematical diffraction from one incident beam.

As regards the realisation of the technique, once theory had pointed it out, Cockayne and Ray worked together on the Elmiskop 1 to put it into practice. It should be remembered that at that time electron microscopes had been designed with the biological user's needs primarily in mind, with bright-field axial beam imaging, and with only single axis specimen tilt for stereo imaging. A Valdrè double-tilt specimen holder had become available, but considerable effort and ingenuity were required to achieve results. Ray was involved in specimen preparation, and both worked together to tilt the incident beam to the orientation required to excite a weak-beam

on the microscope axis. Getting the correct photographic plate exposure, with long exposure times, and minimising specimen stage drift were all difficulties to be overcome. It was a considerable achievement on the part of both of them.

3. Applications

Those illustrated are necessarily selective, and micrographs are invariably at 100 keV beam potential.

3.1 Silicon

An early application was to the improvement of dislocation structure revealed by going from strong-beam imaging to weak-beam imaging (Ray and Cockayne [7]). Figures 5(a) and (b) are a pair of strong-beam and weak-beam images of a silicon specimen taken with a strong 220 type Bragg reflection (figure 5(a)) and with the corresponding weak-beam condition (figure 5(b), $|s| > 2x10^{-2}$ Å^{-1}). The weak-beam image shows a great increase in detail visible, including dissociation into partial dislocations. Dissociation of three-fold nodes into extended intrinsic and extrinsic nodes was also observed. Such dissociation disproved an earlier suggestion of Booker and Brown [8] that dislocations in silicon were unextended. Figure 6 is a further example of the improvement for a dislocation line in silicon, showing: (a) a strong-beam 220 type image; (b) undissociated and dissociated segments taken with the 220 type reflection weak; (c) an image taken with a 111 type reflection such that $\mathbf{g}.\mathbf{b} = 0$ for the undissociated segments, which are therefore invisible, while the dissociated segments are made visible by the contrast due to the strip of stacking fault; (d) an image taken with a 220 type reflection which renders one of the partial dislocations bounding the dissociated segments invisible. An extended 3-fold node is also visible. The configuration is most likely due to a dislocation climbing at a shallow angle to its glide plane with dissociated segments in the glide plane and undissociated segments climbing out of the glide plane.

Figure 6(c) is interesting from an historical point of view. The interest in our group in Cambridge for entering the electron microscope field was generated by some early electron micrographs of beaten gold foil taken with a Metropolitan-Vickers EM3 electron microscope [9]. Streaks on selected area electron diffraction patterns indicated the presence of stacking faults, while electron micrographs showed areas with dark bands parallel to the traces of {111} planes. Peter Hirsch had the idea that such bands might be due to inclined stacking faults cutting through the foil causing a difference in phase of $2\pi\,\mathbf{g}.\mathbf{R}$ between electron waves scattered from opposite sides of the fault. Peter Hirsch pointed this out to the author when he joined his group as a research student in 1954, and said that because of this phase difference,

dislocations might be made visible when they are dissociated into stacking fault ribbons. The idea was just a hunch, with details of the stacking fault contrast remaining to be worked out. Nevertheless, it was a crucial idea. At that time metallurgists and electron microscopists did not hold out any hope of seeing dislocations directly with the electron microscope. Their contrast ideas were focussed on density changes, which they thought would be too small to cause any effect. The contrast due to the phase $2\pi\,\mathbf{g}.\mathbf{R}$ has been called Bragg diffraction phase contrast. Peter Hirsch was a member of the Crystallographic Laboratory of the Cavendish Laboratory, and such a phase effect was well known to X-ray crystallographers.

The first (recognised) observations of dislocations in aluminium [10] showed that even an undissociated dislocation is made visible by diffraction contrast due to the continuous strain field of a dislocation. The stacking fault ribbon is not necessary. At the same time Bollmann [11, 12] obtained images of both dislocations and stacking faults in stainless steel. But it is interesting to note that figure 6(c) illustrates Peter Hirsch's hunch of 1954. For more detail on the history of the subject see reference [13].

3.2 Further early applications

(a) **Stacking fault energies of f.c.c. metals.** The partial dislocation separations for silver and copper have been measured for various orientations between edge and screw dislocations (Cockayne, Jenkins and Ray [14]). Figure 7 shows results for silver, from which a stacking fault energy γ of 16.3 ± 1.7 *erg* cm^{-2} was derived. Similar measurements for copper gave a value for γ of 41 ± 9 *erg* cm^{-2}. Carter and Ray [15] made similar studies for copper alloys (Cu + Al, Cu + Ge, Cu + Si, Cu + Zn) both from partial dislocation separations and (for some) from node shapes. This and various data from other sources led to a plot of γ versus the *e/a* ratio.

(b) **Observation of constrictions on dissociated dislocations.** Carter and Ray [15] studied copper 7 at .% silicon alloy. Interesting weak-beam micrographs were obtained, of which figure 8 is typical showing constrictions presumably at jogs on dissociated dislocations. The motion of the constrictions was studied using a high-temperature specimen stage at ~300°C. Figure 8 (at 20°C) shows that one partial of the dissociated dislocation is more flexible at the constriction than the other partial. The more flexible partial is near edge orientation, while the other less flexible partial is closer to screw orientation. This difference in flexibility is well known from theory (Brown [16]), where the line tension of a dislocation is given by $E(\theta) + E''(\theta)$, $E(\theta)$ being the line energy as a function of orientation θ. The movement of constrictions along a dislocation at high temperature was observed with a high-temperature specimen stage.

(c) **Superlattice dislocations in ordered Fe Al alloys.**

Ray, Crawford and Cockayne [17. 18] applied the weak-beam technique to ordered Fe Al alloys, where two types of ordering referred to as B2 and DO_3 can occur. The B2 (Fe Al) ordering leads to a unit cell with Fe atoms occupying corner sites of the bcc Fe lattice, with Al atoms at the body-centre sites, while DO_3 (Fe_3 Al) has a unit cell eight times the volume of that of bcc Fe. Two-fold dissociation of dislocations into partials with anti-phase boundaries in B2 was observed, while four-fold dissociation in DO_3, with appropriate anti-phase boundaries separating the partials, was observed with the weak-beam technique. Figure 9 is an interesting example in the DO_3 structure showing zig-zag shapes of the partials near edge orientation due to the instability predicted by Head [19]. Anti-phase boundary energies were derived for orientations between edge and screw character.

(d) The weak-beam technique has also been applied to the study of small interstitial Frank loops in silicon formed by irradiation with P^+ ions (Jenkins, Cockayne and Whelan [20]). Loops in the 100Å diameter size range were well imaged, but smaller loops (< 50 Å diameter) were not so clearly imaged. Small Guinier-Preston zones in aluminium-copper alloys have also been studied with the weak-beam technique (Yoshida, Cockayne and Whelan [21]).

3.3 **Weak-beam contrast asymmetry for stacking faults**

This topic has led to some considerable investigation, experimental and theoretical, since the first reported unusual (i.e. unexpected) contrast effects for weak-beam images of stacking faults in germanium and silicon of Cullis and Booker [22], followed by similar reports of others. Intrinsic and extrinsic nodes in Ge showed a reversal of the averaged contrast with reversal of s for fixed **g**, while intrinsic stacking faults in Si showed a reversal of the averaged contrast with reversal of **g**, s remaining the same in sign. The kinematical theory of stacking fault images of Whelan and Hirsch [23] leads to no background intensity asymmetry for the averaged contrast of an intrinsic fault by reversal of **g** or s, i.e. change of sign of $(\mathbf{g}.\mathbf{R})s$. A similar result holds for an extrinsic fault provided its thickness can be neglected. But an extrinsic fault has a finite thickness because it is equivalent to two intrinsic faults on adjacent {111} planes, and for weak-beam conditions the depth periodicity of the intensity of the beam tends to $1/s$. For s sufficiently large, the periodicity is comparable with the thickness of the fault, and this needs to be taken into account in the kinematical theory. A treatment so based was given by Föll, Carter and Wilkens [24], which suggested that an extrinsic fault would exhibit contrast asymmetry with change of sign of $(\mathbf{g}.\mathbf{R})s$. This was confirmed by a quantitative study of Cockayne et al [25].

The situation for an intrinsic fault is not so clear. The kinematical theory predicts no asymmetry for an intrinsic fault with reversal of the sign of (**g**.**R**)*s*, contrary to what was observed [22, 24, 25]. Even for an intrinsic fault, electronic bond redistribution at the fault is to be expected, so that the fault region might appear to have a thickness. Calculations using multislice diffraction theory [26] have revealed a contrast asymmetry for an intrinsic fault. The situation was described by Cockayne [27] as remaining to be fully exploited.

4 Concluding remarks

From what has been mentioned in this short review, it is clear that the weak-beam technique pioneered by David Cockayne and Ian Ray has led to significant advances in the study of materials.

I wish to thank Professor Cockayne for many stimulating discussions over more than forty years.

References

[1] T. Mulvey, Biographical Memoirs of Fellows of the Royal Society **40** 61 (1994).

[2] P.B. Hirsch, A. Howie and M.J. Whelan, Phil. Trans. Roy. Soc. London A **252** 499 (1960). See also reference [3] chapter 7.

[3] P.B. Hirsch, A. Howie, R.B. Nicholson, D.W. Pashley and M.J. Whelan, In: *Electron Microscopy of Thin Crystals,* Butterworths, London, (1965) chapters 4, 7.

[4] D.J.H. Cockayne, J.R. Parsons and C.W. Hoelke, Phil. Mag. **24** 139 (1971).

[5] D.J.H. Cockayne, I.L.F. Ray and M.J. Whelan, Phil. Mag. **20** 1265 (1969).

[6] D.J.H. Cockayne, Journal of Microscopy **98** Part 2, 116 (1973).

[7] I.L.F. Ray and D.J.H. Cockayne, Proc. Roy. Soc. London A **325** 543 (1971).

[8] G.R. Booker and L.M. Brown, Phil. Mag. **11** 1315 (1965).

[9] P.B. Hirsch, A. Kelly and J.W. Menter, In: *Proceedings of the Third International Conference on Electron Microscopy,* London, Royal Microscopical Society, 231 (1954).

[10] P.B. Hirsch, R.W. Horne and M.J. Whelan, Phil. Mag. **1** 677 (1956).

[11] W. Bollmann, Phys. Rev. **103** 1588 (1956).

[12] W. Bollmann, In: *Report of First European Regional Conference on Electron Microscopy,* Stockholm, Almqvist and Wiksell, 316 (1957).

[13] M.J. Whelan, Journal of Electron Microscopy Technique **3** 109 (1986).

[14] D.J.H. Cockayne, M.L. Jenkins and I.L.F. Ray, Phil. Mag. **24** 1383 (1971).

[15] C.B. Carter and I.L.F. Ray, Phil.Mag. **29** 1231 (1974).

[16] L.M. Brown, Phil. Mag **10** 441 (1964).

[17] I.L.F. Ray, R.C. Crawford and D.J.H. Cockayne, Phil. Mag. **21** 1027 (1970).

[18] R.C. Crawford, I.L.F. Ray and D.J.H. Cockayne, Phil. Mag. **27** 1 (1973).

[19} A.K. Head, Phys. Stat. Sol. **19** 185 (1967).

[20] M.L.Jenkins, D.J.H. Cockayne and M.J. Whelan, Journal of Microscopy **98** Part 2, 155 (1973)

[21] H. Yoshida, D.J.H. Cockayne and M.J. Whelan, Phil. Mag. **34** 89 (1976).

[22] A.G. Cullis and G.R. Booker, In: Proceedings of the Fifth European Congress on Electron Microscopy, The Institute of Physics, London and Bristol, 532 (1972).

[23] M.J. Whelan and P.B. Hirsch, Phil.Mag. **2** 1121, 1303 (1957).

[24] H. Föll, C.B. Carter and M. Wilkens, Phys. Stat. Sol. **58 a** 393 (1980).

[25] D.J.H. Cockayne, P. Pirouz, Z. Liu, G.R. Anstis and P. Karnthaler, Phys. Stat. Sol. **82 a** 425 (1984).

[26] A.R. Wilson and D.J.H. Cockayne, Phil. Mag. **51** 341 (1985).

[27] D.J.H. Cockayne, In: *Topics in Electron Diffraction and Microscopy,* The Institute of Physics Publishing, Bristol and Philadelphia, (1999) chapter 2.

The development and early applications of the weak-beam technique

M.J. Whelan

Captions to figures

Figure 1. Intensity profiles of images of a screw dislocation for various values of n = **g**.**b**. The actual image intensity for unit incident beam intensity is the ordinate multiplied by $(2\xi_g s)^{-2}$, where ξ_g is the extinction distance for the Bragg reflection. See reference [3] for definition of ξ_g. The core of the dislocation is at $\beta = 0$. Note that the image peak lies to one side of the dislocation core.

From Hirsch et al. [2]. Courtesy of the Royal Society.

Figure 2. $2\bar{2}0$ weak-beam image of a dislocation near edge orientation (**b** = $\frac{1}{2}[1\bar{1}0]$) in Cu + 10 at .% Al alloy with $s_{\bar{2}20} \simeq 0$. The diffraction pattern inset shows encircled the weak-beam reflection used for the image. The two image peaks demonstrate dissociation into partial dislocations.

From Cockayne et al. [5]. Courtesy of the Philosophical Magazine.

Figure 3. Computed $2\bar{2}0$ image profile for a dissociated edge dislocation in Cu, for a separation of partial dislocations of $50\,\overset{0}{\text{A}}$ and with $s_{\bar{2}20} = 0$. Foil thickness is $870\,\overset{0}{\text{A}}$, depth of the dislocation $430\,\overset{0}{\text{A}}$.

From Cockayne et al. [5]. Courtesy of the Philosophical Magazine.

Figure 4. Weak-beam diffraction geometries. In (a) the reflection + **g** is strongly excited and the image is formed with the weak systematic reflection - **g**. In (b) 3**g** is strongly excited and the image is formed with the weak beam **g**. In (c) no strong reflection is excited.

Figure 5 (a), (b).
(a) $2\bar{2}0$ strong beam image of dislocations in deformed silicon. (b) Corresponding weak-beam $2\bar{2}0$ image of the same area showing greatly improved resolution of detail. The diffraction patterns inset show the imaging beams encircled.

From Ray and Cockayne [7]. Courtesy of the Royal Society.

Figure 6(a)-(d). Constricted and dissociated segments along a dislocation line in silicon imaged for various diffraction conditions.
(a) $2\bar{2}0$ strong-beam image, where the dislocation structure is poorly resolved. (b) $2\bar{2}0$ weak-beam image showing partial dislocations at dissociated segments. (c) $11\bar{1}$ weak-beam image with $\mathbf{g}.\mathbf{b} = 0$ for the undissociated segments, which are therefore invisible. For the extended node at the left and the dissociated segments the contrast is due to the stacking fault. (d) $0\bar{2}2$ weak-beam image for which one of the partials with Burgers vector $\frac{1}{6}[2\bar{1}\bar{1}]$ 07/09/2009 is out of contrast.

From Ray and Cockayne [7]. Courtesy of the Royal Society.

Figure 7. Experimental measurement of partial dislocation separation Δ as a function of dislocation line orientation θ in silver. The curves are computed using anisotropic elasticity theory. The dashed lines indicate the separations derived from a Peierls mode of the dislocation core. Stacking fault energies γ are indicated.

From Cockayne et al. [14]. Courtesy of the Philosophical Magazine.

Figure 8. Constrictions along a dissociated dislocation in Cu + 7 at .% Si alloy after annealing at 320° C in a heating specimen holder. The weak-beam image, taken with a $2\bar{2}0$ reflection, for which **g** and **b** for the various dislocations are indicated.

From Carter and Ray [15]. Courtesy of the Philosophical Magazine.

Figure 9. Weak-beam image of a dislocation in Fe-26 at.% Al alloy with DO_3-type long range order, showing four-fold dissociation into partials. Anisotropic elasticity theory shows that there is an instability orientation range from 105° to 156° (measured anticlockwise from [111]), which is circumvented by the partials adopting a zig-zag configuration.

From Crawford et al. [18]. Courtesy of the Philosophical Magazine.

Figure 1

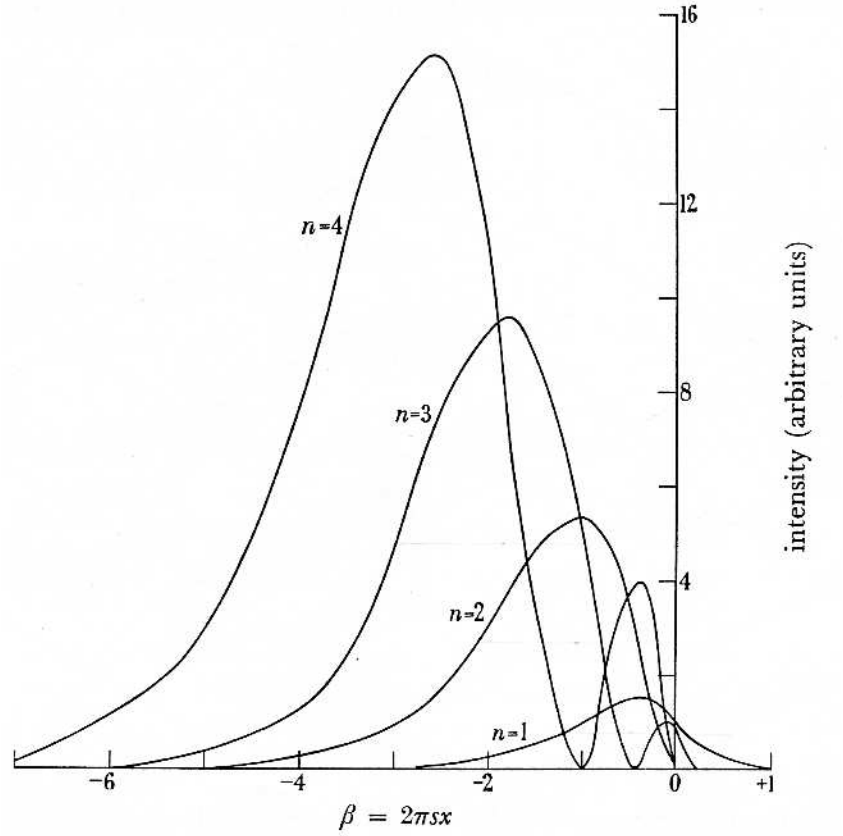

Figure 2

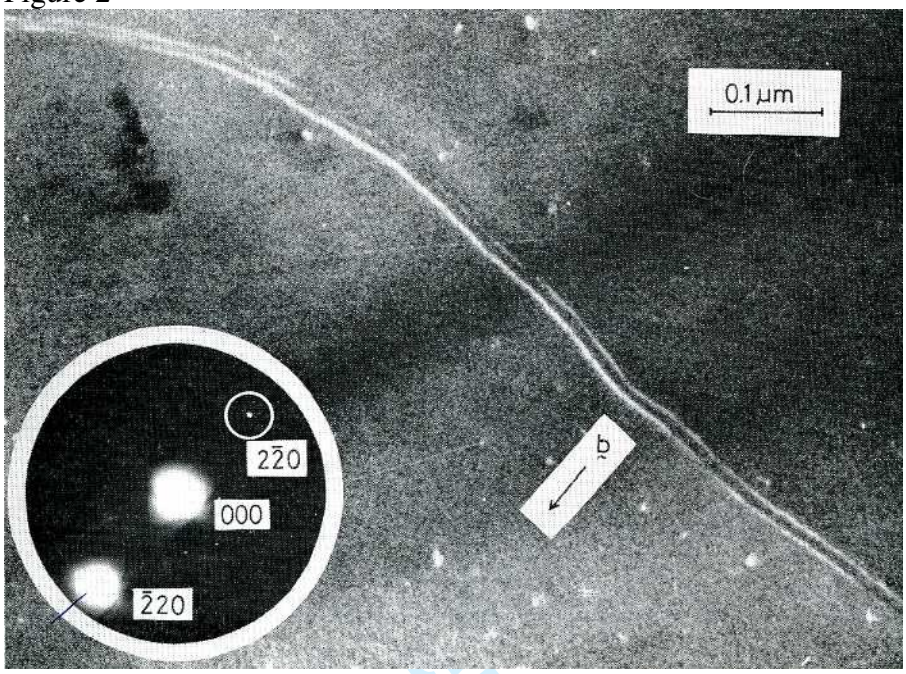

Figure 3

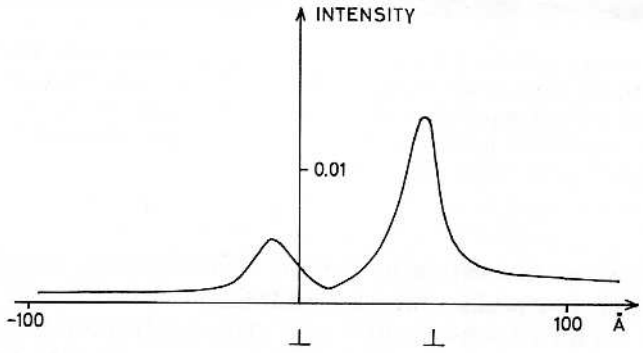

Figure 4

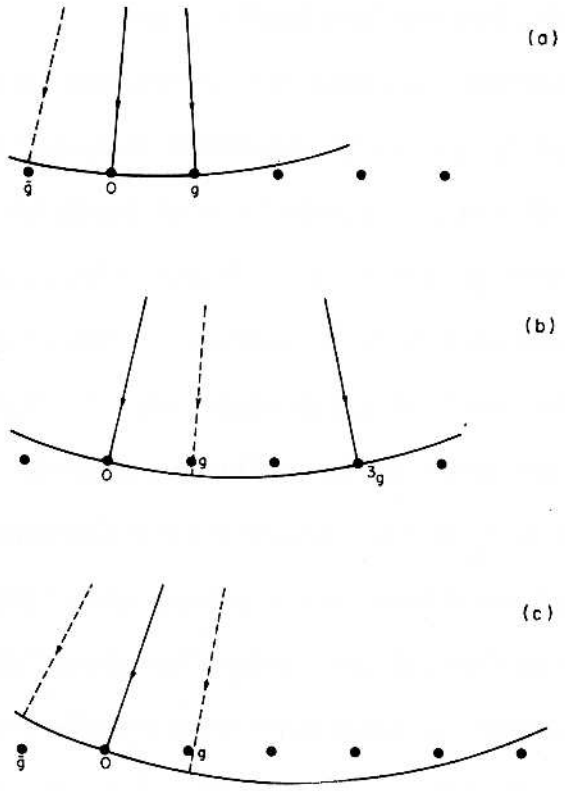

Figure 5a

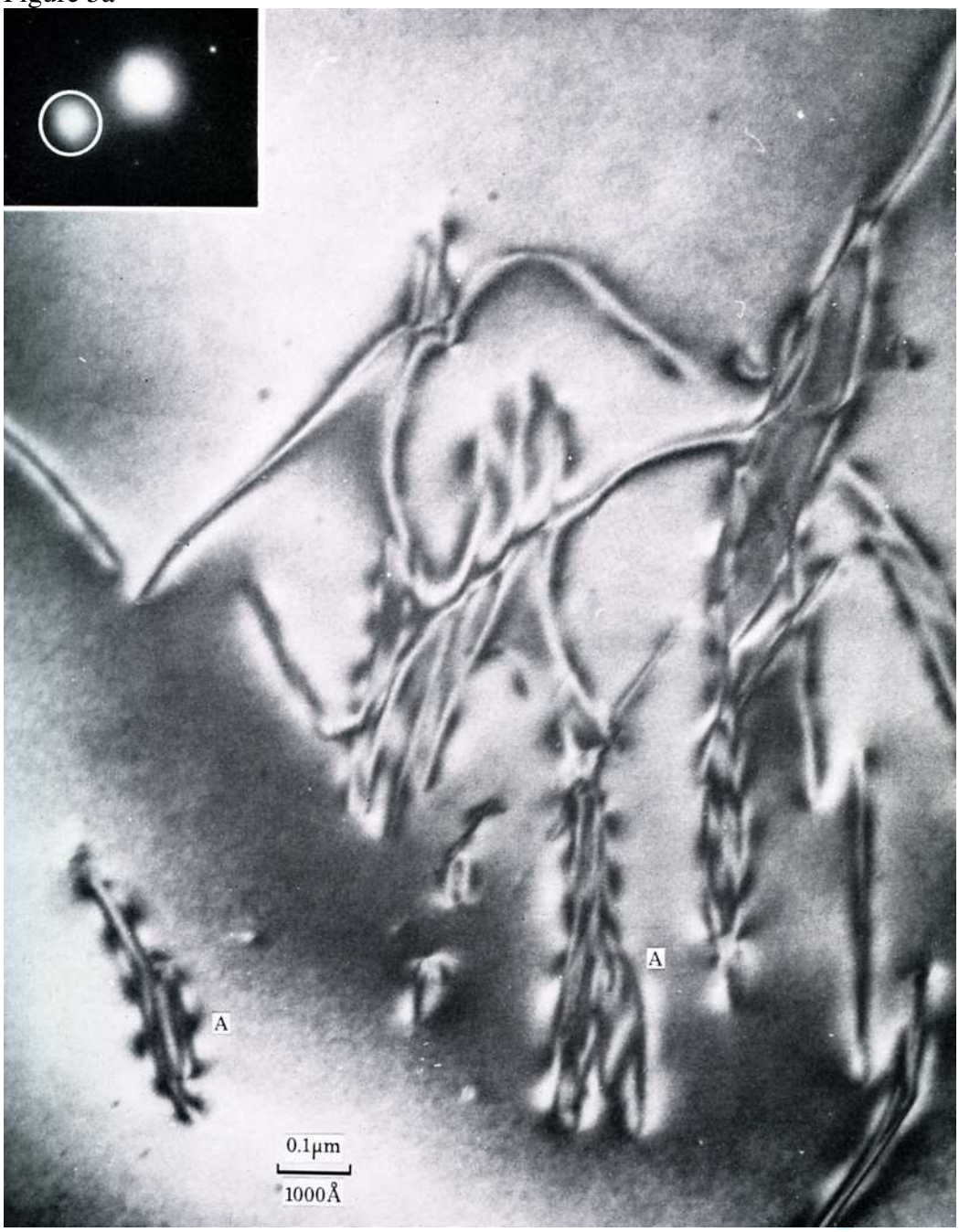

Figure 5b

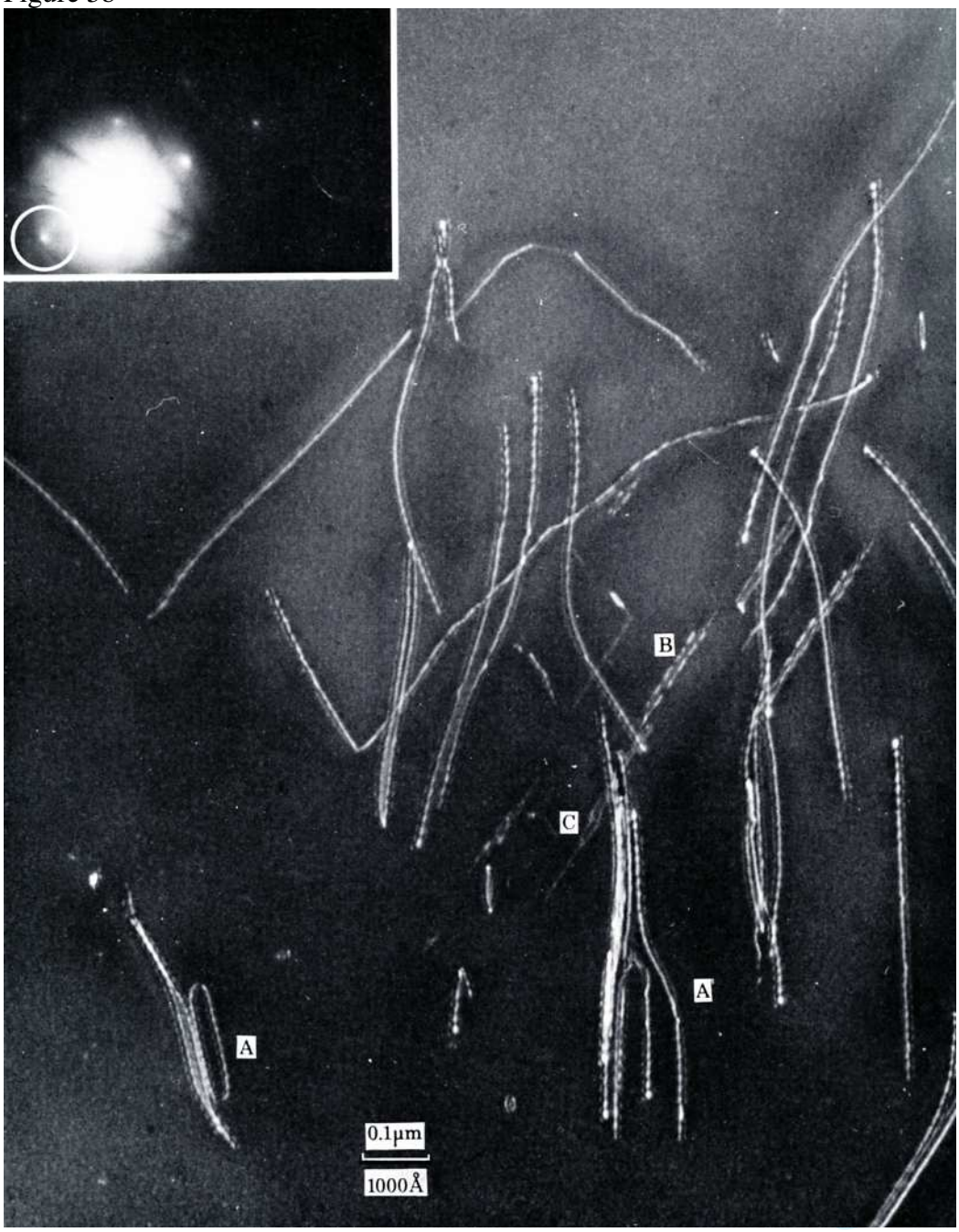

Figure 6

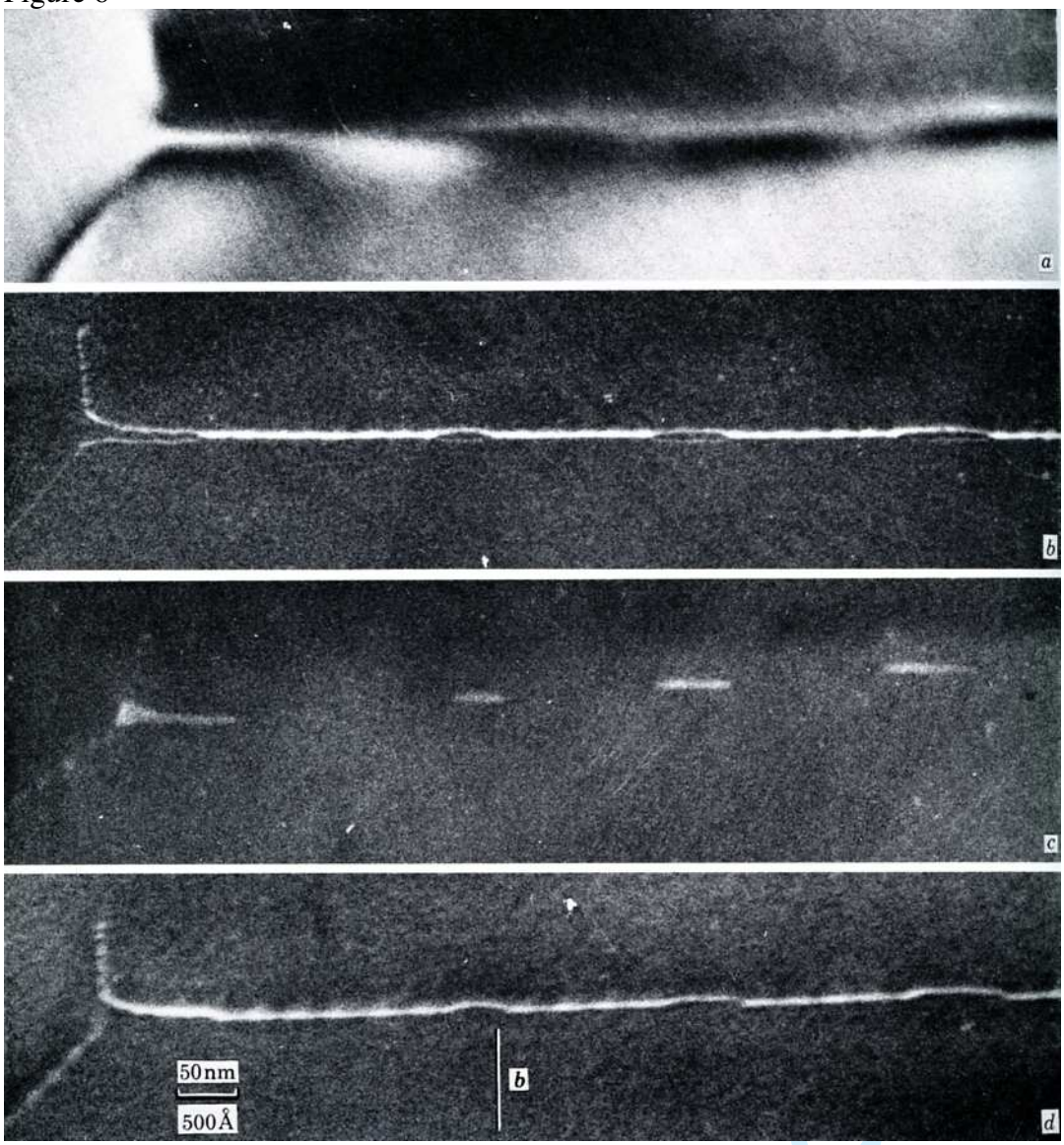

Figure 7

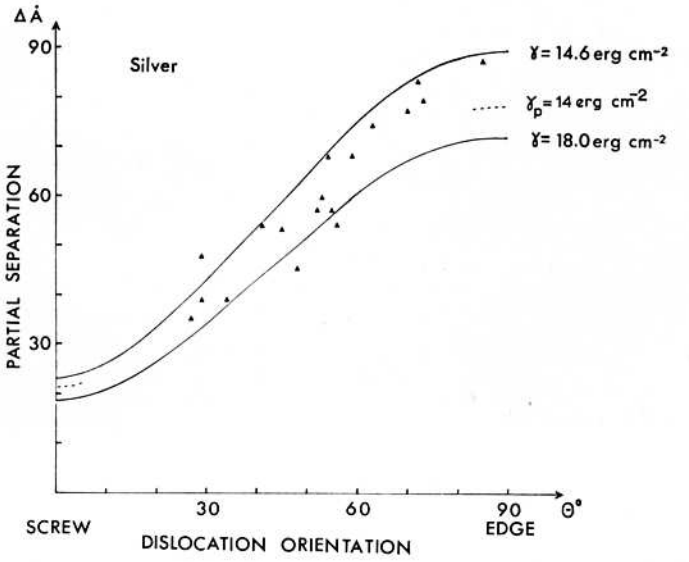

Figure 8

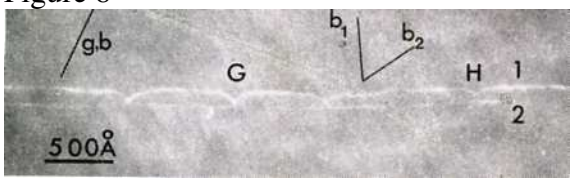

Figure 9